INTERNATIONAL JOURNAL FOR NUMERICAL AND ANALYTICAL METHODS IN GEOMECHANICS
Int. J. Numer. Anal. Meth. Geomech., **22**, 603–619 (1998)

RATIONAL APPROXIMATION OF STRESS AND STRAIN BASED ON DOWNHOLE ACCELERATION MEASUREMENTS

R. O. DAVIS* AND J. B. BERRILL

Department of Civil Engineering, University of Canterbury, Christschurch, New Zealand

SUMMARY

Recordings from downhole accelerometer arrays offer unique insight into soil behavior and ground response during earthquakes. In this paper we present a scheme for interpolating displacement and acceleration measurements to provide approximations for subsurface shear strain and stress as continuous functions of time. Our suggested interpolating functions are constructed in such a way that the free surface boundary condition will always be satisfied and the interpolated displacement and acceleration remain finite for all depths. We also show how the functions can be adapted to represent layered soil profiles. Depending on the number of instruments in the downhole array, a truncated series of functions can be derived so that each represents a modal shape for the layered soil profile. The resulting approximations for strain and stress are considered more accurate and robust than previous approximations. © 1998 John Wiley & Sons, Ltd.

Key words: earthquakes; stress-strain response; downhole arrays

INTRODUCTION

Downhole accelerometer arrays have been installed in a number of locations around the world and a growing number of records have been obtained from real earthquakes.[1–5] One proposed use for these records is the direct estimation of stress and strain in the ground during the earthquake.[6–10] By approximating stress and strain at different times in the recorded motion, one may create a picture of changes in shear modulus which accompany shaking.

Existing stress and strain estimates for downhole records are based, so far as we know, on simple linear interpolations. Consider the typical situation illustrated in Figure 1. Suppose acceleration records a_A and a_B from two instruments denoted A and B have been obtained. These records are integrated to give the ground displacements u_A and u_B. All of the quantities a_A, a_B, u_A and u_B are functions of time. The usual approximations for stress τ and strain γ at any particular time t are

$$\begin{aligned} \tau(x,t) &= \int_0^x \rho a(x,t)\,\mathrm{d}x \approx \frac{\rho}{h_B - h_A}\left[(a_A h_B - a_B h_A)x + \frac{1}{2}(a_B - a_A)x^2\right] \\ \gamma(x,t) &= \frac{\partial u(x,t)}{\partial x} \approx \frac{u_B - u_A}{h_B - h_A} \end{aligned} \tag{1}$$

* Correspondence to: R. O. Davis, Department of Civil Engineering, University of Canterbury, Christchurch, New Zealand

CCC 0363–9061/98/080603–17$17.50

Received 11 July 1997
Revised 13 October 1997

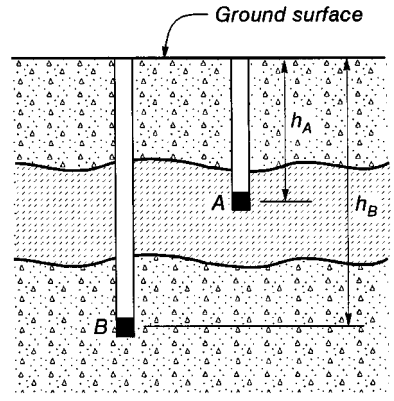

Figure 1. A typical downhole array consisting of two instruments denoted A and B

Here ρ denotes the soil density, x the depth, and h_A and h_B are the depths of the two instruments.

Both approximations result from linear interpolation. In the case of the stress τ, the acceleration is interpolated between the two depths and then integrated. In the case of the strain γ, the displacement is interpolated and the slope measured. The accelerations a_A and a_B, and the displacements u_A and u_B, are evaluated at time t. If more than two instrument records are available, these representations might be altered somewhat, but the basic idea of linear interpolation would be retained.

The central theme of this paper is to provide more robust and accurate approximations than those shown above. Approximations of the form shown in equation (1) can be viewed as the simplest possible measures of stress and strain based on instrumental records. In particular, the shear strain given by (1) can correctly be applied only at the mid-depth between the two accelerometers. A more effective analysis should provide reasonable approximations of both stress and strain at any point in the soil column and additionally should be compatible with known boundary conditions. In the work below we propose the use of trigonometric interpolating functions for both displacements and accelerations. These interpolating functions will permit us to approximate stress and strain at any depth. The resulting approximations for stress and strain will automatically accommodate both the free surface, zero stress boundary condition as well as deliver bounded stresses and strains as depth increases. An additional advantage will also become apparent. We will derive a relatively simple model for layered site response, and it will be used to adjust the calculations for stress and strain in an appropriate way. We will illustrate the method by analysing the Port Island record from the Kobe earthquake.

ANALYSIS FOR HOMOGENEOUS SOIL

While it is possible to consider layered soils, the development for a homogeneous site is simpler and will illustrate the central points of our method. We postpone consideration of layered sites until later in the paper. Here we consider a homogeneous soil profile in which a downhole accelerometer array has been placed. Let the instruments be denoted $A, B, \ldots, J$ in order of increasing depths $h_A, h_B, \ldots$, etc.

Also let $u(x, t)$ denote horizontal displacement and $\ddot{u}(x, t)$ horizontal acceleration in the particular orientation of the instrumental record with which we are concerned. We will identify the specific acceleration at instrument λ by a_λ, $\lambda = A, B, \ldots, J$. The corresponding displacement will be u_λ.

At any particular depth h the shear strain and stress are given by

$$\gamma(h, t) = \frac{\partial u(h, t)}{\partial x}$$
$$\tau(h, t) = \int_0^h \rho \ddot{u}(x, t)\, \mathrm{d}x \tag{2}$$

We will use equations (2) together with appropriate interpolation functions for displacement and acceleration to solve for the strain and stress at any particular time t.

A variety of interpolation functions are available to us. While linear interpolation possesses the advantage of simplicity, the free-surface boundary condition can never be satisfied, and hence we discard it. Polynomials of degree two or higher do have the ability to satisfy the boundary condition at $x = 0$, but they will generally become unbounded as x increases. A third possibility, and the one we pursue here, is a trigonometric series. In particular, a cosine series will automatically satisfy the free surface boundary condition and will remain finite as $x \to \infty$. Thus, we introduce the following interpolating functions for displacement and acceleration:

$$u(x, t) = \beta_0 + \beta_1 \cos \kappa x + \beta_2 \cos 2\kappa x + \cdots + \beta_{J-1} \cos(J-1)\kappa x$$
$$\ddot{u}(x, t) = \alpha_1 \cos \kappa x + \alpha_2 \cos 2\kappa x + \cdots + \alpha_J \cos J\kappa x \tag{3}$$

The number of terms for each series is J, the number of downhole instruments. The coefficients α_λ, β_λ are functions of time. They will be determined by the instantaneous values of measured displacement and acceleration. The inclusion of the coefficient β_o in the displacement expansion where no similar term appears in the acceleration series occurs for reasons to be explained below. Note the presence of one additional arbitrary constant, the wave number κ. We will suggest an appropriate range of values for κ shortly.

Determination of the coefficients in (3) is a straightforward matter. To illustrate, consider the acceleration series. To determine the coefficients α_λ we have the following set of J equations:

$$\begin{bmatrix} c_{1A} & c_{2A} & \cdots & c_{JA} \\ c_{1B} & c_{2B} & \cdots & c_{JB} \\ \vdots & & & \\ c_{1J} & c_{2J} & \cdots & c_{JJ} \end{bmatrix} \begin{bmatrix} \alpha_1 \\ \alpha_2 \\ \vdots \\ \alpha_J \end{bmatrix} = \begin{bmatrix} a_A \\ a_B \\ \vdots \\ a_J \end{bmatrix} \tag{4}$$

Here

$$c_{\lambda N} = \cos \lambda \kappa h_N, \quad \lambda, N = 1, 2, \ldots, J \tag{5}$$

It is a simple matter to solve (4) for the vector of coefficients α_λ. Having done so, the shear stress at any depth h is obtained from (2). Carrying out the integration we find

$$\tau(h, t) = \frac{\rho}{\kappa}\left[\alpha_1 \sin \kappa h + \frac{1}{2}\alpha_2 \sin 2\kappa h + \cdots + \frac{1}{J}\alpha_J \sin J\kappa h\right] \tag{6}$$

A similar development for strain gives

$$\gamma(h, t) = -\kappa[\beta_1 \sin \kappa h + 2\beta_2 \sin 2\kappa h + \cdots + (J-1)\beta_{J-1} \sin(J-1)\kappa x] \tag{7}$$

where the coefficients β_λ are determined by an equation similar to (4) with a vector of measured displacements instead of accelerations.

Before ending this section, we discuss one other detail. Following equation (3) we noted that the strain approximation contained a constant term β_o while no equivalent term is found in the stress approximation. The reason for this is to ensure the strain approximation will approach zero for rigid-body deformation. We can illustrate this point by considering how the approximation works in the simple case of harmonic excitation of a linearly elastic soil column. For vertically propagating harmonic SH waves, the horizontal displacement $u(x, t)$ is given by

$$u(x, t) = u_o(e^{ikx} + e^{-ikx})e^{i\omega t} \tag{8}$$

Here u_o denotes the wave amplitude, ω is the circular frequency of excitation, and k is the excitation wave number (not to be confused with the approximation wave number κ), given by

$$k = \frac{\omega}{c} \tag{9}$$

where c denotes the shear wave velocity. Equation (8) satisfies both the equation of motion and the free-surface boundary condition at $x = 0$. The two exponentials inside the paranthesis represent upward and downward propagating waves. Both waves must have the same amplitude because of the free-surface boundary condition. It will be more convenient to rewrite equation (8) as

$$u(x, t) = 2u_o \cos kx \, e^{i\omega t} \tag{10}$$

Now suppose we have a two-instrument array subject to the motion specified in (10). The strain approximation is easily found from equation (7):

$$\gamma(h, t) = \frac{-\kappa \sin \kappa h(u_B - u_A)}{(c_{1B} - c_{1A})} \tag{11}$$

where u_A and u_B are obtained from (10) with x set equal to h_A and h_B. In the limit as $\omega \to 0$, we have $u_A \to u_B$, and hence $\gamma \to 0$, the expected result for rigid translation. If, on the other hand, the constant coefficient β_0 had not been used in equation (3), then (11) would be replaced by

$$\gamma(h, t) = \frac{-\kappa[c_{2B}u_A - c_{2A}u_B)\sin \kappa h + (c_{1A}u_B - c_{1B}u_A)\sin 2\kappa h]}{c_{1A}c_{2B} - c_{1B}c_{2A}}$$

Now, in the limit as $\omega \to 0$, we find γ will not, in general, vanish. Clearly, (11) is the better approximation based on behaviour for low-frequency excitation. A similar problem does not arise for the acceleration approximation since, in the zero-frequency limit, the elastic accelerations all go to zero.

EXAMPLE: KOBE EARTHQUAKE — HOMOGENEOUS CASE

To illustrate our ideas we will consider the ground motion measurements obtained in the Port Island downhole array from the Kobe earthquake.[3] In this section we treat the Port Island soil

profile as though it were homogeneous. Later the results will be reconsidered in light of soil layering. A central concern in this section will be selection of appropriate values for the approximation wave number κ.

The downhole array at Port Island consisted of four three-component accelerometers at depth 0, 16, 32 and 83 m. Figure 2 shows the recorded accelerations for the east-west component together with the integrated displacement time histories. We will focus attention on the first major acceleration pulse which occurs roughly between 13·5 and 14·5 s on this record.

To begin we have shown in Figure 3 graphs of stress versus strain at two depths, 12 and 23 m, obtained from equations (6) and (7) and based on all four downhole records. The illustrated calculations were carried out with a value of $0{\cdot}02\ \mathrm{m}^{-1}$ for the wave number κ. In selecting this value for κ we are mindful that the best approximation we can hope for can only represent that part of the input wave spectrum with wavelengths on the order of the spacing between downhole instruments or longer. High-frequency, short-length waves cannot be approximated by an array of widely spaced instruments, just as the Nyquist frequency limits the analysis of high-frequency time-series data. Since the wave number is 2π times the reciprocal of wavelength, these comments suggest we use a small value for κ corresponding to a long wavelength. It should not be too small however, else there will be no advantage in using the cosine series. Because of these reasons, we suggest a two-step procedure for selection of κ. We first choose a trial value for κ based on the greatest instrument depth being roughly a quarter wavelength. That is

$$\kappa = \frac{2\pi}{4(h_D - h_A)} = \frac{\pi}{2 \times 83} \approx 0{\cdot}02\ \mathrm{m}^{-1} \tag{12}$$

The second step compares $J\kappa$ with what we will refer to as the Nyquist wave number, namely 2π divided by twice the smallest instrument spacing. For the Port Island array the Nyquist wave number is

$$\kappa_N = \frac{2\pi}{2(h_B - h_A)} = \frac{\pi}{16} \approx 0{\cdot}20\ \mathrm{m}^{-1}$$

If the value of $J\kappa$ is smaller than κ_N, we accept the trial value for κ; otherwise, we reduce κ to some value smaller than κ_N/J. For the Port Island array we have $J\kappa = 4 \times 0{\cdot}02 = 0{\cdot}08\ \mathrm{m}^{-1} < \kappa_N$, hence the original trial value is acceptable. This procedure is based on the idea that the interpolating cosine series can be looked upon as an expansion of eigenfunctions representing the modes of shearing vibration for a homogeneous soil layer with depth equal to the greatest instrument spacing. The first term, with wave number κ, represents the fundamental mode, while the higher terms represent higher modes. The wave number of the highest mode, $J\kappa$, should not exceed the Nyquist wave number in order to avoid spurious information being introduced by the interpolating functions.

What will be the effect if we change κ? Making κ smaller appears to have relatively minor effects as is shown in Figure 4 where similar calculations of stress and strain are illustrated for $\kappa = 0{\cdot}005\ \mathrm{m}^{-1}$ (dashed line) and $\kappa = 0{\cdot}02\ \mathrm{m}^{-1}$ (solid line). We have effectively quadrupled the approximation wave length, but the change in both the stress and strain approximations appears small. In fact the approximations are more different than first appears as illustrated in Figure 5 where the interpolated displacement profiles for the two cases are graphed. These profiles correspond to a time of 14·0 s on the instrumental records, the time at which the maximum stress is attained at the 12 m depth. The ' + ' signs mark the measured values of displacement from the downhole instruments. While the two calculations are similar in the upper 32 m, they differ

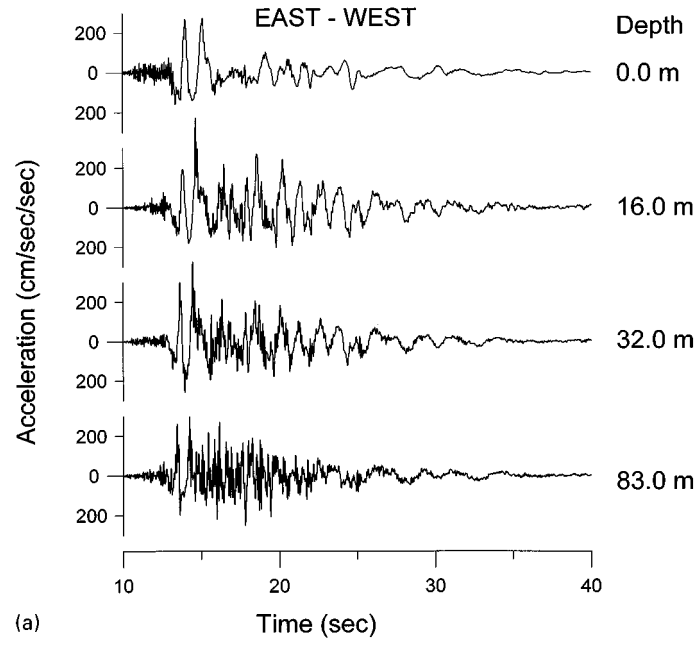

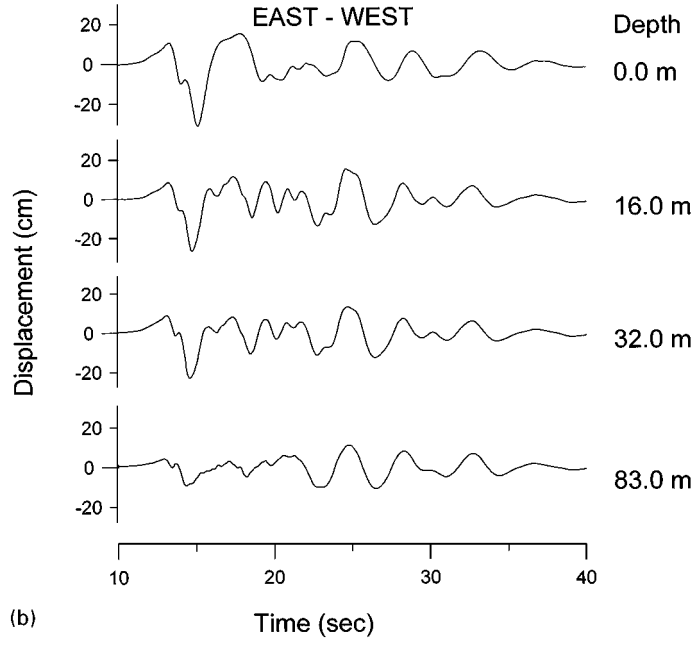

Figure 2. Time histories of acceleration (Part a) and displacement (Part b) from the Port Island downhole array

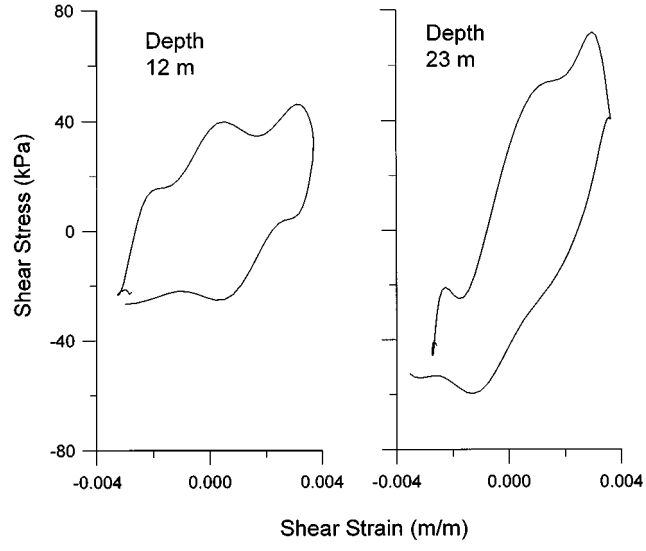

Figure 3. Stress–strain response at two depths based on the Port Island records

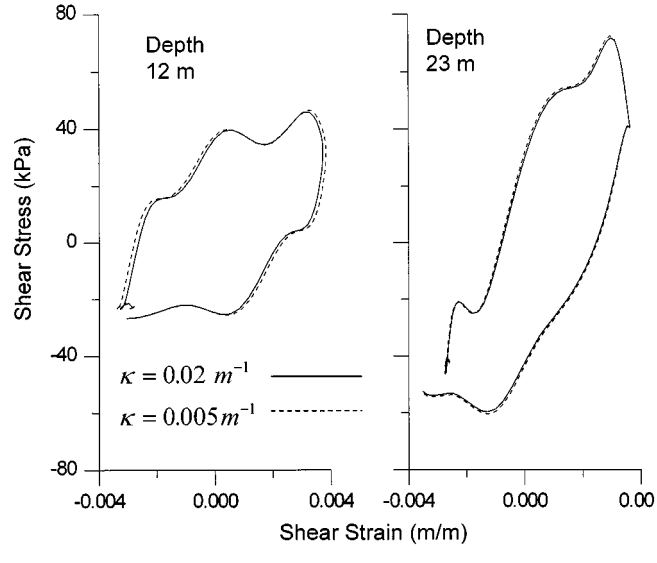

Figure 4. Comparison of approximated stress–strain response for values of the approximation wave number κ equal to 0·005 m^{-1} (dashed line) and 0·02 m^{-1} (solid line)

markedly at greater depths. This figure clearly demonstrates the lack of control over the approximated displacements when the instruments are more widely dispersed.

If we increase κ, there will naturally be a risk of introducing short wave length information into our approximations when it is not justified to do so. To illustrate consider Figure 6. Here we see

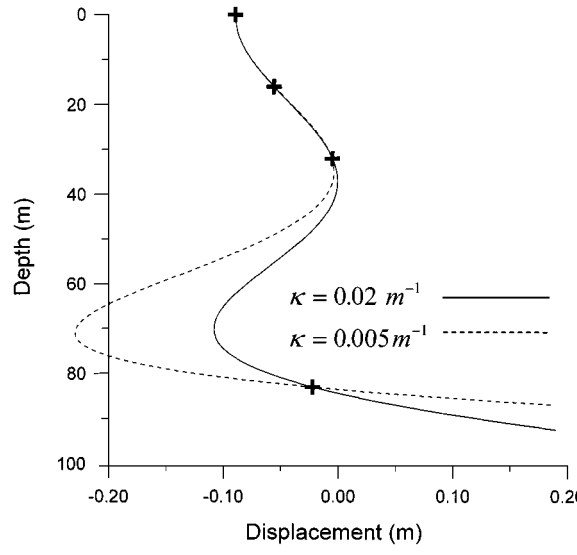

Figure 5. Profile of interpolated displacement versus depth for two values of κ. The ' + ' signs denote the four measured displacements

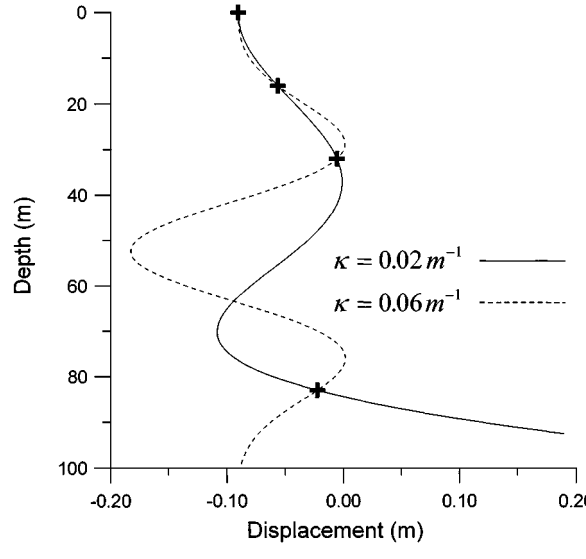

Figure 6. Displacement profiles similar to Figure 5 but showing the effect of a larger value for κ

the displacement profile at 14 s for $\kappa = 0{\cdot}06\ \mathrm{m}^{-1}$. This calculation clearly contains a greater high-frequency content than the data will support. The stress–strain curves corresponding to Figures 3 and 4 are not shown, but they are significantly different from the calculations with $\kappa = 0{\cdot}02$ and $0{\cdot}005\ \mathrm{m}^{-1}$.

Clearly, the stress and strain approximations will be sensitive to be value chosen for κ. The displacement profiles of Figures 5 and 6 represent conditions at only one time in the recordings, but the same general conclusions apply for literally any other time. Selection of κ is a matter of judgement, although the form given in (12) has been found to work well in most circumstances. The development here also emphasises the importance of the instrument spacing in a downhole array. Widely spaced instruments will not in general yield useful approximations for stress and strain, regardless of what level of sophistication is employed in their analysis.

We can also compare the result from our analysis with the approximations contained in equations (1). For the 12 m depth we can use equations (1) as they stand, based on the upper two instrument records. For the 23 m depth both equations are modified to account for the third instrument in the array. Instead of (1) we use

$$\tau(h,t) = \frac{\rho}{h_B - h_A}\left[(a_A h_B - a_B h_A)h_B + \frac{1}{2}(a_B - a_A)h_B^2\right] + \frac{\rho}{h_C - h_B}\left[(a_B h_C - a_C h_B)(h - h_B) + \frac{1}{2}(a_C - a_B)(h^2 - h_B^2)\right]$$

$$\gamma(x,t) = \frac{u_C - u_B}{h_C - h_B}$$

Here the stress approximation results from integrating the linearly interpolated accelerations from the ground surface to the depth h. The linear approximations for stress and strain at both the 12 and 23 m depths at time 14·0 s are shown by the dashed lines in Figure 7. For comparison,

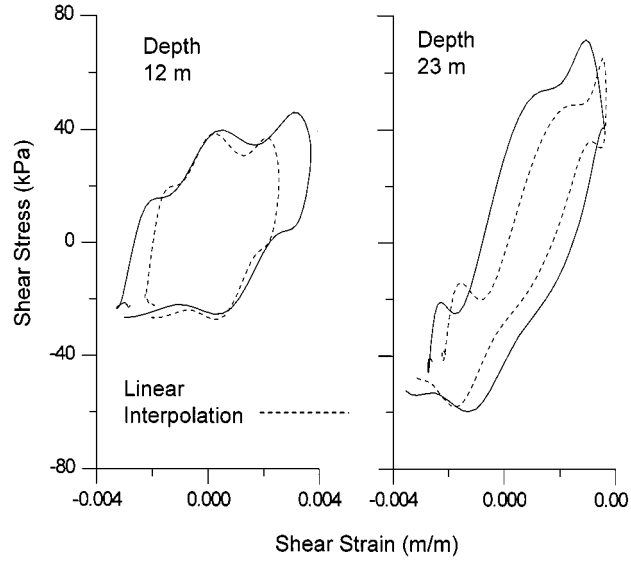

Figure 7. Comparison of stress–strain response: The four term trigonometric approximation is shown by the solid line, the linear approximation shown by the dashed line

approximations based on equations (6) and (7) with $\kappa = 0{\cdot}02\ \mathrm{m}^{-1}$ are also shown as solid lines on this figure. The two approximations are vaguely similar, but, especially at the 12 m depth, there are significant differences in the magnitude of strain. The reason behind this difference is immediately evident from inspection of Figure 5. If we were to sketch a straight line joining the measured displacements marked by + signs, then the linear approximation would suggest the strain at all depths between '+'s will be given by the slope of the line. Obviously, this is not an especially strong approximation for strain, particularly near the ground surface or near the depth of any instrument. To be fair, most recent applications of the linear method have specified the strains should only be evaluated at the midpoint between instruments. This will obviously improve their accuracy, but restrict their utility.

ANALYSIS FOR LAYERED SOILS

The full power embedded in the cosine series approximation does not become evident until we consider a layered soil site. Let the soil profile be as indicated in Figure 8. We see a sequence of horizontal layers numbered downward from the ground surface. The thickness of layer m is denoted h_m and the density and shear wave velocity of the layer are given by ρ_m and c_m. As will be seen shortly, it is not necessary to know in advance the value of c_m, but it will be necessary to estimate the impedance ratios $\rho_m c_m/\rho_n c_n$ for all layers before solving for stresses and strains.

We begin by constructing a local coordinate frame for layer m. The depth h is measured from the upper surface of the layers as shown in Figure 8. In order to analyse the layered-soil problem, it will be useful to consider harmonic waves propagating vertically in the soil profile. For any given frequency, this is equivalent to considering the Fourier components of a more general wave form. Let u_m and τ_m denote the Fourier components of displacement and shear stress for frequency $\lambda\omega$ evaluated at the upper surface of the layer. The corresponding displacement and stress at depth

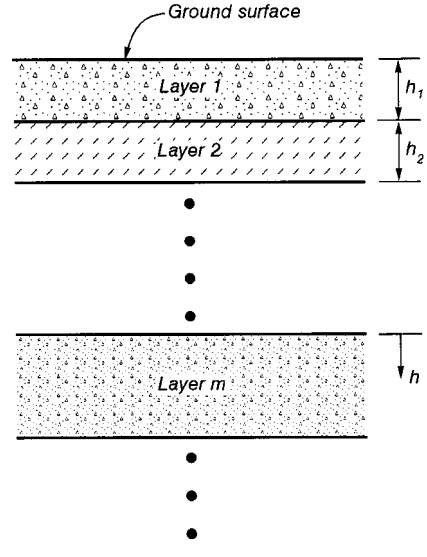

Figure 8. A typical layered soil profile

h are given by

$$\begin{Bmatrix} u(h,t,m) \\ \tau(h,t,m) \end{Bmatrix} = [\mathbf{H}_m] \begin{Bmatrix} u_m \\ \tau_m \end{Bmatrix} \tag{13}$$

Here $\mathbf{H}_m$ represents the Haskell–Thomson transfer matrix[11]

$$\mathbf{H}_m = \begin{bmatrix} \cos \lambda\kappa_m h & \dfrac{1}{\lambda\omega\rho_m c_m} \sin \lambda\kappa_m h \\ -\lambda\omega\rho_m c_m \sin \lambda\kappa_m h & \cos \lambda\kappa_m h \end{bmatrix} \tag{14}$$

and the wave number κ_m is given by

$$\kappa_m = \omega / c_m.$$

Shortly, we will let λ take on values 0, 1, 2,... giving a discrete sequence of frequencies from which expressions similar to those in equation (3) can be constructed. Note the explicit dependence on layer m shown on the left-hand side of equation (13).

In the special case of the uppermost layer ($m = 1$), equation (13) gives

$$u(h,t,1) = u_1 \cos \lambda\kappa_1 h, \quad 0 \leqslant h \leqslant h_1 \tag{15}$$

Here u_1 denotes the Fourier component of displacement at the ground surface and we have used the zero-stress boundary condition $\tau_1 = 0$. In the analysis below we will interpret the displacement u_1 as a coefficient β_λ of one of the terms in a series similar to the cosine series for displacement in equation (3).

The most useful aspect of the transfer matrix is that we can multiply matrices for successive layers to obtain the displacement at any point in the soil profile. That is, we can rewrite (13) as the product of m matrices

$$\begin{Bmatrix} u(h,t,m) \\ \tau(h,t,m) \end{Bmatrix} = [\mathbf{H}_m][\mathbf{H}_{m-1}] \cdots [\mathbf{H}_1] \begin{Bmatrix} u_1 \\ 0 \end{Bmatrix} \tag{16}$$

This equation relates the displacement and shear stress in layer m to the displacement and the *zero* shear stress at the ground surface. The matrices $\mathbf{H}_{m-1}, \mathbf{H}_{m-2}, \ldots, \mathbf{H}_1$ are evaluated with h equal to the appropriate layer thickness $h_{m-1}, h_{m-2}, \ldots, h_1$. In the matrix $\mathbf{H}_m$, of course, h can take on any value between 0 and h_m. Now, we can easily use (16) to build up the displacement in any layer. For example, in layer 2 we have

$$u(h,t,2) = u_1 \cos \lambda\kappa_1 h_1 \cos \lambda\kappa_2 h - u_1 \frac{\rho_1 c_1}{\rho_2 c_2} \sin \lambda\kappa_1 h_1 \sin \lambda\kappa_2 h, \quad 0 \leqslant h \leqslant h_2 \tag{17}$$

while in layer 3

$$\begin{aligned} u(h,t,3) = {} & u_1 \cos \lambda\kappa_1 h_1 \cos \lambda\kappa_2 h_2 \cos \lambda\kappa_3 h \\ & - u_1 \frac{\rho_1 c_1}{\rho_2 c_2} \sin \lambda\kappa_1 h_1 \sin \lambda\kappa_2 h_2 \cos \lambda\kappa_3 h \\ & - u_1 \frac{\rho_2 c_2}{\rho_3 c_3} \cos \lambda\kappa_1 h_1 \sin \lambda\kappa_2 h_2 \sin \lambda\kappa_3 h \\ & - u_1 \frac{\rho_1 c_1}{\rho_3 c_3} \sin \lambda\kappa_1 h_1 \cos \lambda\kappa_2 h_2 \sin \lambda\kappa_3 h \end{aligned} \tag{18}$$

The entire displacement profile can be constructed in this manner moving down through each layer successively. Note that in each of the expressions above h is measured from the upper surface of the relevant layer.

Next, fix the value of the frequency ω and consider the expressions above as λ takes on values $0, 1, 2, \ldots$. Let $c_{\lambda h}^{m}$ represent the combination of terms that multiply u_1 in the expression for the displacement $u(h, t, m)$. That is, for $m = 1$,

$$c_{\lambda h}^{1} = \cos \lambda \kappa_1 h, \quad \kappa_1 = \omega / c_1 \tag{19}$$

which follows from (15). Similarly, for $m = 2$, we have from (17)

$$c_{\lambda h}^{2} = \cos \lambda \kappa_1 h \cos \lambda \kappa_2 h - \frac{\rho_1 c_1}{\rho_2 c_2} \sin \lambda \kappa_1 h_1 \sin \lambda \kappa_2 h, \quad \kappa_m = \omega / c_m \tag{20}$$

Then we can approximate the entire displacement profile with a series of the form

$$u(h, t, m) = \beta_0 + \beta_1 c_{1h}^{m} + \beta_2 c_{2h}^{m} + \cdots \tag{21}$$

where the coefficients $\beta_0, \beta_1, \beta_2, \ldots$ will be determined by the measured displacements from the downhole instrument records. We can look upon each of the functions $c_{\lambda h}^{m}$ as a modal shape. The coefficients β_λ are weightings which physically represent the ground surface displacement u_1 corresponding to each mode.

Now suppose one instrument of a downhole array lies in layer m. Let the instrument be identified by A and let h_A denote the position of the instrument in the layer measured from the layer surface. Then let $c_{\lambda A}^{m}$ represent the function $c_{\lambda h}^{m}$ with h replaced by h_A so that

$$u_A = u(h_A, t, m) = u_1 c_{\lambda A}^{m} \tag{22}$$

where we have used u_A to represent the measured value at time t from the downhole array. Next, suppose we have an array of instruments $A, B, \ldots, J$ placed in soil layers $m_A, m_B, \ldots, m_J$. Then we can approximate the complete displacement field with a truncated series of the form

$$u(h, t, m) = \beta_0 + \beta_1 c_{1h}^{m} + \beta_2 c_{2h}^{m} + \cdots + \beta_{J-1} c_{(J-1)h}^{m} \tag{23}$$

where the coefficients β_λ are determined by solving this set of equations

$$\begin{bmatrix} 1 & c_{1A}^{m_A} & c_{2A}^{m_A} & \cdots & c_{(J-1)A}^{m_A} \\ 1 & c_{1B}^{m_B} & c_{2B}^{m_B} & \cdots & c_{(J-1)B}^{m_B} \\ \vdots & & & & \\ 1 & c_{1J}^{m_J} & c_{2J}^{m_J} & \cdots & c_{(J-1)J}^{m_J} \end{bmatrix} \begin{Bmatrix} \beta_0 \\ \beta_1 \\ \vdots \\ \beta_{J-1} \end{Bmatrix} \sim \begin{Bmatrix} u_A \\ u_B \\ \vdots \\ u_J \end{Bmatrix} \tag{24}$$

Once the coefficients β_λ have been determined for a particular value of t, the strain at any depth h in any layer m immediately follows from

$$\gamma(h, t, m) = \left[\frac{\partial u(x, t, m)}{\partial x} \right]_{x=h} = \left[\beta_1 \frac{\partial c_{1h}^{m}}{\partial x} + \beta_2 \frac{\partial c_{2h}^{m}}{\partial x} + \cdots + \beta_{J-1} \frac{\partial c_{(J-1)h}^{m}}{\partial x} \right]_{x=h} \tag{25}$$

To illustrate, suppose we have a situation with three downhole instruments. For any particular time t we use equation (24) to find the coefficients β_λ. Then for a point in layer 1 we have the simple result

$$\gamma(h, t, 1) = -\beta_1 \kappa_1 \sin \kappa_1 h - 2\beta_2 \kappa_1 \sin 2\kappa_1 h \tag{26}$$

and this equation applies for $0 \leqslant h \leqslant h_1$. In layer 2 we have

$$\begin{aligned} \gamma(h, t, 2) = & -\beta_1 \kappa_2 \left(\cos \kappa_1 h_1 \sin \kappa_2 h + \frac{\rho_1 c_1}{\rho_2 c_2} \sin \kappa_1 h_1 \cos \kappa_2 h \right) \\ & -2\beta_2 \kappa_2 \left(\cos 2\kappa_1 h_1 \sin 2\kappa_2 h + \frac{\rho_1 c_1}{\rho_2 c_2} \sin 2\kappa_1 h_1 \cos 2\kappa_2 h \right) \end{aligned} \tag{27}$$

which applies for $0 \leqslant h \leqslant h_2$. Similar expressions are easily obtained for layers 3, 4, etc.

We can follow a parallel development to find the shear stress. First, we need to approximate the acceleration profile in the layered soil. This can be done with a transfer matrix approach similar to (13). Focusing on accelerations, the appropriate equation for layer m involves acceleration and stress

$$\begin{Bmatrix} \ddot{u}(h, t, m) \\ \tau(h, t, m) \end{Bmatrix} = [\mathbf{L}_m] \begin{Bmatrix} \ddot{u}_m \\ \tau_m \end{Bmatrix} \tag{28}$$

where the transfer matrix $\mathbf{L}_m$ is given by

$$\mathbf{L}_m = \begin{bmatrix} \cos \lambda \kappa_m h & -\dfrac{\lambda^2 \omega^2}{\rho_m c_m} \sin \lambda \kappa_m h \\ (\lambda \omega)^{-2} \rho_m c_m \sin \lambda \kappa_m h & \cos \lambda \kappa_m h \end{bmatrix} \tag{29}$$

As before, we can multiply successive transfer matrices in order to relate the acceleration in layer m to that at the ground surface.

$$\begin{Bmatrix} \ddot{u}(h, t, m) \\ \tau(h, t, m) \end{Bmatrix} = [\mathbf{L}_m][\mathbf{L}_{m-1}] \cdots [\mathbf{L}_1] \begin{Bmatrix} \ddot{u}_1 \\ 0 \end{Bmatrix} \tag{30}$$

Then in layer 1 the acceleration is

$$\ddot{u}(h, t, 1) = \ddot{u}_1 \cos \lambda \kappa_1 h, \quad 0 \leqslant h \leqslant h_1 \tag{31}$$

while in layer 2

$$\ddot{u}(h, t, 2) = \ddot{u}_1 \cos \lambda \kappa_1 h_1 \cos \lambda \kappa_2 h - \ddot{u}_1 \frac{\rho_1 c_1}{\rho_2 c_2} \sin \lambda \kappa_1 h_1 \sin \lambda \kappa_2 h, \quad 0 \leqslant h \leqslant h_2 \tag{32}$$

An equation similar to (18) occurs for layer 3. Note that the collection of terms that multiply the surface acceleration $\ddot{u}_1$ are the same as the coefficients $c_{\lambda h}^m$ which arose in the development for displacements.

Now we can approximate the complete acceleration profile with a series similar to (23),

$$\ddot{u}(h, t, m) = \alpha_1 c_{1h}^m + \alpha_2 c_{2h}^m + \cdots + \alpha_{J-1} c_{(J-1)h}^m \tag{33}$$

where the coefficients α_λ are obtained from the measured accelerations by solving

$$\begin{bmatrix} c_{1A}^{m_A} & c_{2A}^{m_A} & \cdots & c_{(J-1)A}^{m_A} \\ c_{1B}^{m_B} & c_{2B}^{m_B} & \cdots & c_{(J-1)B}^{m_B} \\ \vdots & & & \\ c_{1J}^{m_J} & c_{2J}^{m_J} & \cdots & c_{(J-1)J}^{m_J} \end{bmatrix} \begin{Bmatrix} \alpha_1 \\ \alpha_2 \\ \vdots \\ \alpha_{J-1} \end{Bmatrix} = \begin{Bmatrix} a_A \\ a_B \\ \vdots \\ a_J \end{Bmatrix} \tag{34}$$

Note that no constant term α_0 is required here.

Finally, we obtain the shear stress by integrating the accelerations. A separate integral is required for each layer:

$$\tau(h, t, m) = \int_0^{h_1} \rho_1 \ddot{u}(x, t, 1)\, dx + \int_0^{h_2} \rho_2 \ddot{u}(x, t, 2)\, dx + \cdots + \int_0^{h} \rho_m \ddot{u}(x, t, m)\, dx \tag{35}$$

Once again suppose three downhole records are available. Then for a particular time t we can determine the coefficients $\alpha_1, \alpha_2, \alpha_3$ from equation (34). The stress in layer 1 will be given by

$$\tau(h, t, 1) = \frac{\rho_1}{\kappa_1}\left(\alpha_1 \sin \kappa_1 h + \frac{\alpha_2}{2} \sin 2\kappa_1 h + \frac{\alpha_3}{3} \sin 3\kappa_1 h\right) \tag{36}$$

In layer 2 we have

$$\begin{aligned} \tau(h, t, 2) = {} & \frac{\rho_1}{\kappa_1}\left(\alpha_1 \sin \kappa_1 h_1 + \frac{\alpha_1}{2} \sin 2\kappa_1 h_2 + \frac{\alpha_3}{3} \sin 3\kappa_1 h_1\right) \\ & + \frac{\rho_2 \alpha_1}{\kappa_2}\left(\cos \kappa_1 h_1 \sin \kappa_2 h - \frac{\rho_1 c_1}{\rho_2 c_2} \sin \kappa_1 h_1 [1 - \cos \kappa_2 h]\right) \\ & + \frac{\rho_2 \alpha_2}{2\kappa_2}\left(\cos 2\kappa_1 h_1 \sin 2\kappa_2 h - \frac{\rho_1 c_1}{\rho_2 c_2} \sin 2\kappa_1 h_1 [1 - \cos 2\kappa_2 h]\right) \\ & + \frac{\rho_2 \alpha_3}{3\kappa_2}\left(\cos 3\kappa_1 h_1 \sin 3\kappa_2 h - \frac{\rho_1 c_1}{\rho_2 c_2} \sin 3\kappa_1 h_1 [1 - \cos 3\kappa_2 h]\right) \end{aligned} \tag{37}$$

Expressions for subsequent layers become longer but no additional real difficulties arise.

We can use equations (25) and (35) to estimate the stress and strain in the layered soil at any particular time t. In comparison to the homogeneous soil case, some additional information is required concerning the various soils. Naturally, an estimate for the density of each layer ρ_m is needed. The model is not particularly sensitive to ρ_m and in many instances a constant value for all layers would probably be sufficient. More important are the values for the impedance ratios $\rho_m c_m / \rho_n c_n$ between the various layers. These values must be specified in advance and they play an important role in determining the modal shapes $c_{\lambda h}^m$ in all layers below the uppermost layer. It is not necessary to specify the stiffness or the shear wave velocity for any individual layer. We must select an appropriate value for one of the wave numbers κ_λ depending on the depth at which the stress and strain approximations are desired and the spacing of instruments. The other wave numbers then follow from the impedance ratios and the assumed densities. The layered model appears to be moderately insensitive to the values of the wave numbers (as was the case for the

homogeneous model) provided reasonable values are used. Aside from these points the only other information needed are values for the thickness of each layer. Naturally, as the number of layers increases, so will the amount of algebra, but the equations are easily handled by machine.

EXAMPLE 2: KOBE EARTHQUAKE — LAYERED ANALYSIS

Our second example calculation will again involve records from the Port Island downhole array. A somewhat idealized soil profile for Port Island is shown in Figure 9. In fact, the uppermost 19 m of the soil consisted of four similar layers of gravel and gravelly sand. See Reference 3 for details. The clay layer between 19 and 27 m is considered to be locally homogeneous, but the sands and gravels below 27 m were also layered and showed slightly differing properties. Nevertheless, the profile illustrated in Figure 9 roughly accounts for the main features of the site and is sufficiently simple to permit relatively easy calculations. Also shown in Figure 9 are estimated values for the impedance ratios between the three layers. We have used an assumed density of 1·80 t/m^3 in all layers.

Figure 10 shows the approximated stress–strain response covering the same time frame as in Figures 3 and 4 and at the same depths. The solid line shows the response of the layered model. The dashed line is the homogeneous soil response, identical to Figure 3. At the 12 m depth the two curves are so close as to be nearly indistinguishable. At 23 m, however, there are significant differences in the magnitude of strain. This depth of course lies at the centre of the clay layer. Profiles of both acceleration and displacement corresponding to 14·0 s are shown in Figure 11. Again the result for the homogeneous model is shown as a dashed line. Recalling that the clay layer extends from 19 to 27 m, it is clear the layered-model responds quite differently in this region. Note that both displacement and acceleration profiles have discontinuous spatial derivatives at the interfaces between the layers. The differences between the homogeneous and layered

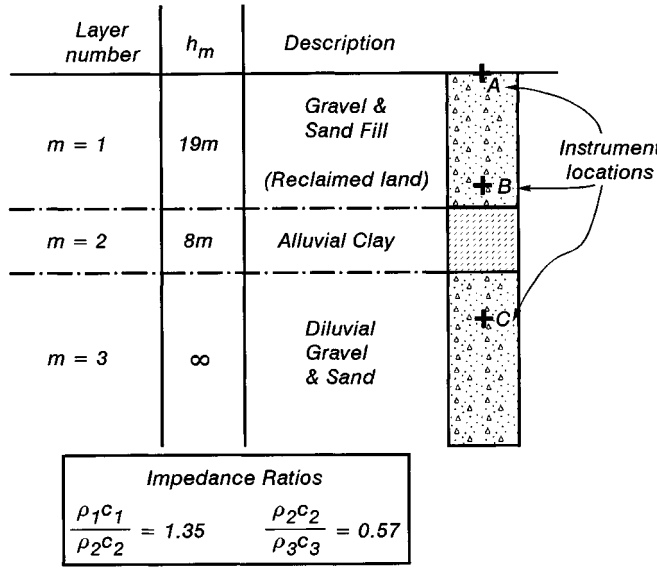

Figure 9. Three-layer idealisation of the Port Island soil profile. Impedance ratios between the layers are shown in the box

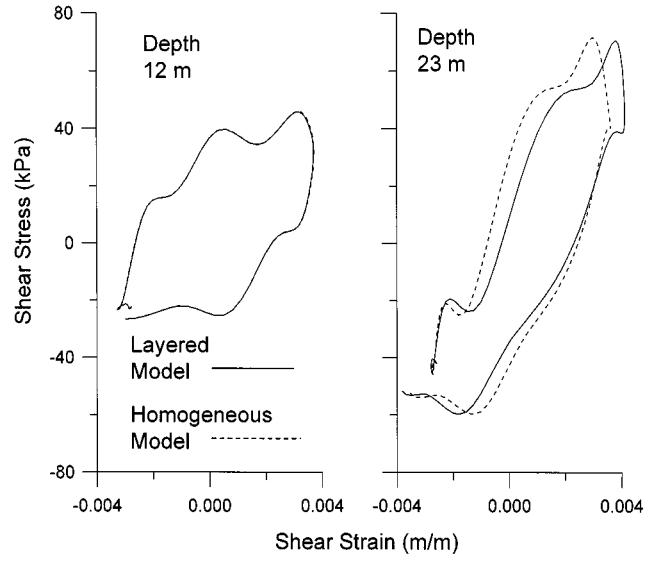

Figure 10. Comparison of stress–strain response: layered soil response is shown by the solid line, homogeneous soil response is the dashed line

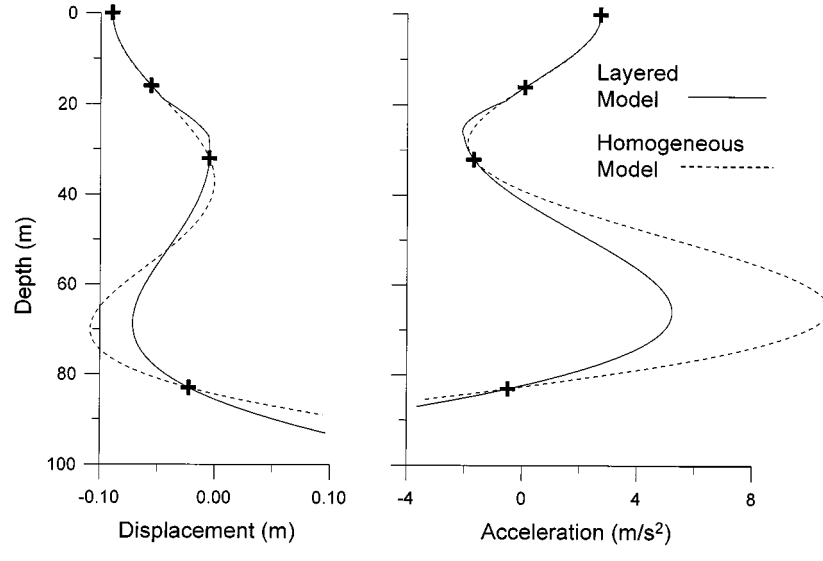

Figure 11. Profiles of interpolated displacement and acceleration for the layered-soil model (solid line) and the homogeneous model (dashed line)

models may be put into perspective by assessing the apparent shear moduli of the two hysteresis loops at the 23 m depth in Figure 10. If we simply connect the maximum and minimum stress points with a straight line and calculate the slope we find a modulus of 22·3 MPa for the layered response compared to a modulus of 28·6 MPa for the homogeneous response, a relative difference of more than 20 per cent.

CONCLUSIONS

In this paper we have explored ways to approximate shear stresses and strains based on strong motion data from downhole accelerometer arrays. Trigonometric series appear to have considerable potential as interpolating functions for both acceleration and displacement. They will automatically satisfy the boundary conditions associated with the free surface as well as ensuring the approximating functions remain bounded as depth increases. The trigonometric series are basically no more difficult to work with than the linear interpolations which have been used in the past, yet they offer significant advantages of greater accuracy and the ability to represent layered soil profiles. Layering has been introduced in such a way that the only additional information needed is impedance ratios between different soils. Stress and strain follow easily once the interpolation functions are known.

We have also presented a selection of example calculations to illustrate our method. The Kobe earthquake is of considerable interest in its own right, but it is not our object to investigate it in detail here. Instead, we have drawn on relatively small portions of the measured records in an effort to throw light on the proposed appoximation techniques. In a future paper we will investigate the Kobe as well as other downhole records in more detail.

A final point can be made concerning downhole arrays. While any information concerning subsurface soil response is clearly of interest in earthquake engineering, it is apparent that more closely spaced instruments will deliver much higher-quality information. Future installations of downhole instrumentation should be made with this point clearly in mind.

ACKNOWLEDGEMENTS

We thank Dr. Yoshinori Iwasaki and the Committee of Earthquake Observation and Research in the Kansai Area (CEORKA) for making the Port Island records available to us.

REFERENCES

1. S. Iai, T. Morita, T. Kameoka, Y. Matsunage and K. Abiko, 'Response of a dense sand deposit during 1993 Kushiro-Oki Earthquake', *Soils Found.*, **35,** 115–131 (1995).
2. K. Ishihara, T. Muroi and I. Towhata, '*Insitu* Pore water pressures and ground motions during the 1987 Chiba-Toho-Oki Earthquake', *Soils Found.*, **29,** 75–90 (1989).
3. Y. Iwasaki and M. Tai, 'Strong motion records at Kobe Port Island', *Soils Found.*, *Kobe Earthquake Special Issue*, 29–40 (1996).
4. H.-C. Huang and H.-C. Chiu, 'Estimation of site amplification from Dahan Downhole readings', *Earthq. Engng. Struct. Dyn.*, **25,** 319–332 (1996).
5. T. L. Holzer, T. L. Youd and T. C. Hanks, 'Dynamics of liquefaction during the 1987 Superstition Hills, California, earthquake', *Science*, **244,** 56–59 (1989).
6. M. Zegal and A.-W. Elgamal, 'Analysis of site liquefaction using the earthquake records', *J. Geotech. Engng. ASCE*, **120,** 996–1017 (1994).
7. A.-W. Elgamal, M. Zegal and E. Parra, 'Liquefaction of reclaimed island in Kobe, Japan', *J. Geotech. Engng. ASCE*, **122** (1), 39–49 (1996).
8. A.-W. Elgamal, M. Zegal, H. T. Tang and J. C. Stepp, 'Lotung downhole array. I: Evaluation of site dynamic properties', *J. Geotech. Engng. ASCE*, **121,** 350–362 (1995).
9. M. Zeghal, A.-W. Elgamal, H. T. Tang and J. C. Stepp, 'Lotung downhole array. II: Evaluation of soil nonlinear properties', *J. Geotech. Engng. ASCE*, **121,** 363–378 (1995).
10. S. Glaser, 'Insight into liquefaction by system identification', *Geotechnique*, **46,** 641–665 (1996).
11. N. A. Haskell, 'Crustal reflection of plane SH waves', *J. Geophys. Res.*, **65,** 4147–4150 (1960).

